Sensors and Materials, Vol. 36, No. 8 (2024) 3573–3594
MYU Tokyo

S & M 3751

Differences in Applications of Various Neural Network Algorithms for Thermal Error Compensation

Tung-Hsien Hsieh,[1*] Hsin-Yu Lai,[1] Yi-Hao Chou,[2] and Tsai-Hsu Wu[2]

[1]Department of Automation Engineering/Smart Machinery and Intelligent Manufacturing Research Center, National Formosa University, No. 64, Wunhua Rd., Huwei Township, Yunlin County 632301, Taiwan (R.O.C.)
[2]Department of Mechanical Engineering, National Taiwan University, No. 1, Sec. 4, Roosevelt Road, Taipei 10617 Taiwan (R.O.C.)

(Received November 1, 2023; accepted June 10, 2024)

Keywords: thermal deformation of machine tools, neural network, noncontact optical measurement

In traditional machine tool thermal error detection, eddy current or capacitive probes are mainly used. We propose a new data sensing architecture consisting of two main components: a thermal error sensing model and a temperature sensing module. The thermal error sensing model is composed of two quadrant detectors forming a 3D displacement error sensing module. The temperature sensing module consists mainly of multiple PT100 sensors. In the thermal rise experiment, spindle *XYZ* directional thermal errors are detected by the displacement error sensing module, while temperature changes at various locations are detected by the PT100 sensors. The experimental results show that the main thermal errors of the spindle are in the *YZ* direction. Therefore, we introduce four neural network algorithm methods [Temporal Convolutional Network (TCN), Generative Adversarial Network (GAN), Long Short-Term Memory (LSTM), and Bi-directional LSTM (BiLSTM)] to establish various models for predicting the spindle's thermal errors in the *YZ* direction. The predictive results indicate that *Z*-direction predictions are more accurate, with model accuracy maintained up to 70% after six months. In the *Y*-direction thermal error model, significant improvements in prediction results were observed after the RPM parameter was incorporated into the model. Among the various models compared, TCN and BiLSTM show the best performance in terms of accuracy over extended periods and across different thermal error directions.

1. Introduction

Machine tool errors can be classified into three categories: structural, dynamic, and static errors, with thermal error constituting over 50% of the total error. Among these, spindle thermal error is the most significant contributor to thermal error.(1) Thus, thermal error compensation has always been a widely discussed topic. The main development directions for thermal error compensation technology include several areas, such as developing new thermal error measurement methods, creating new sensor selection methods, and developing new thermal

*Corresponding author: e-mail: andycloud@nfu.edu.tw
https://doi.org/10.18494/SAM4747

ISSN 0914-4935
https://myukk.org/

error models. These approaches have demonstrated significant improvements in prediction accuracy and error reduction with the incorporation of neural network algorithms.

In the past, many scholars have experimented with different sensor selection and thermal error measurement methods. Jywe and colleagues proposed an optical five-axis measurement system (LASER R-TEST) that uses a laser and sensors to obtain *X*, *Y*, and *Z* position signals. LASER R-TEST can measure machine tool eccentricity, rotational axis positioning errors, and spindle thermal errors.[2–4] Lu *et al.* used the Spearman correlation coefficient and reduced the number of sensors from 16 to 7.[5] They then established a prediction model using Long Short-Term Memory (LSTM) and General Regression Neural Network (GRNN), resulting in a decrease in RMSE from 4.29 to 1.57 μm.[5] Zheng *et al*. used the Pearson correlation coefficient for temperature feature selection.[6] By using sensor selection methods, the number of sensors can be reduced, thereby lowering the cost of future sensor installations on the machine. Liu *et al.* used variational mode decomposition (VMD), LSTM, and the grey wolf (GW) optimizer to establish a thermal error model.[7] They found that VMD-GW-LSTM was superior to VMD-LSTM and recurrent neural networks (RNNs), with compensation rates of 77.78, 75, and 77.78% for three different sizes.[7] Chen used the Spearman correlation coefficient for sensor selection and established an LSTM-based thermal error model and a compensation method, while the actual cutting residual was 22 μm with compensation thermal error.[8] Liu *et al.* presented a novel method that combines key temperature point (KTP) selection and LSTM modeling for accurate spindle thermal displacement prediction in machine tools.[9] Liu *et al.* introduced a Bi-directional LSTM (BiLSTM) deep learning model for thermal error prediction in computer numerical control (CNC) machining, considerably enhancing machining accuracy and workpiece precision.[10] Zhang *et al.* introduced a Generative Adversarial Network (GAN)-Support Vector Regression method for predicting the angle of tube-bending rebound.[11] They addressed the issue of insufficient data for metal tube-bending samples by using Wasserstein distance in the GAN for data augmentation, resulting in higher prediction accuracy and addressing the problem of gradient vanishing during training.[11] Yoon *et al.* proposed Time GAN, a novel framework that combines supervised and adversarial training to generate realistic time series data.[12] Wu *et al.* proposed a GAN-based framework with piecewise linear representation (PLR) to improve stock prediction by learning trading actions (buying, selling, and holding). PLR forms guided trading sequences for the GAN discriminator, while the GAN generator predicts daily actions. This approach outperforms LSTM networks.[13] Ravuri *et al.* trained a model on a corpus of precipitation events using radar data.[14] Their model allowed for fast, full-resolution nowcasts and outperformed several baselines in predicting meteorologically challenging events.[14]

In contrast, some studies have explored novel methodologies for thermal error prediction. These alternative methods offer diverse perspectives and contribute to the broader understanding of thermal error analysis in manufacturing. Jia *et al.* introduced a novel one-dimensional convolutional neural network (CNN)-gated recurrent unit (GRU)-attention model for spindle thermal error prediction, achieving an accuracy of 81.53% and an RMSE that is 40% lower than those of traditional methods.[15] This model integrates convolutional, GRU, and attention mechanisms for effective feature extraction and error prediction.[15] Kuo *et al.* presented a

machine learning method using a bi-directional GRU neural network optimized by Logistic Random Generator Time-Varying Acceleration Coefficient Particle Swarm Optimization, offering the high-accuracy prediction of thermal displacement in manufacturing.[16] Tan *et al.* developed a CNN and an informer-based model for the accurate temperature prediction of spindle bearings under variable operating conditions.[17] Chen and Wang proposed a method using B-P neural network modeling to predict and compensate for thermal error in NC machining, significantly improving machining accuracy and process capability index (CPK).[18] Similarly, Yin *et al.* introduced a Segment Fusion Least Squares Support Vector Machine method for a more accurate thermal error prediction in CNC machining, which is related to multiple linear regression models (MLR).[19] Guo *et al.* introduced an attention-based CNN model for predicting spindle thermal errors in NC machines, enhancing accuracy and overcoming the Artificial Neural Network's local minimum problem.[20] Wu *et al.* developed a CNN model integrating thermal images and thermocouple data for accurate spindle thermal error prediction in CNC machining.[21] Li *et al.* presented an Improved Binary Grasshopper Optimization Algorithm-feature selection method for identifying temperature-sensitive points in the thermal error modeling of machine tools, enhancing prediction accuracy.[22]

We aim to use temperature sensors and a 3D sensing module to collect input and output data for the spindle thermal error model. We tested two selection mechanisms, the Spearman correlation coefficient and XGBoost, to select feature parameters that are highly correlated with thermal error, eliminate redundant parameters, and then apply neural network algorithm methods to establish thermal error models. The system enables spindle thermal error measurement and model establishment, providing users with higher accuracy and improved competitiveness. The rest of the paper is organized into four sections: Section 2 includes principles of research and the setup and verification of the measurement system. Section 3 delves into data collection, selection mechanisms, and the compensation model. In Sect. 4, the results are analyzed, highlighting improvements made in predicting thermal errors. Lastly, Sect. 5 provides a summary of the key findings.

2. Research Principles, Framework, and Methods

2.1 Principles of research

In this study, the thermal error of a spindle was collected using a 3D sensing module, while temperature data were gathered using a PT100 sensor. The spindle rotational speed was captured through the Internet of Things technology connected to a CNC controller.[1] Then, we used four different neural network algorithm methods (LSTM, BiLSTM, TCN, and GAN) to establish thermal error models. Finally, these thermal error models were utilized to predict the thermal error displacement of the spindle. The following parts will elaborate on the details of the measurement system used.

2.2 LASER R-TEST verification

2.2.1 LASER R-TEST

LASER R-TEST is divided into two parts, as shown in Fig. 1. The first part consists of a 3D sensing module, which utilizes two sets of laser light and two photoelectric quadrant detectors (QDs). The second part comprises a standard rod, which includes a cutter arbor, a metal rod, and a spherical lens. The measurement involves mounting the standard rod on the CNC spindle and aligning the center of the spherical lens in the standard rod with the spindle. Subsequently, the 3D sensing module is installed on the work platform, aligning the intersection point of the two orthogonal laser light sources in the 3D sensing module with the center of the spherical lens. Once the setup is complete, the spherical lens undergoes rotational motion as the spindle rotates. The positional signals for the *X*–*Z* and *Y*–*Z* directions of the center of the spherical lens are individually detected by the two sets of QDs. This method enables the sensing of XYZ coordinate variations during the spindle's rotation.

Currently, the system operates at a sampling frequency of 1 kHz. During sampling, the least squares circle method is employed to accurately calculate the thermal error in the *XYZ* directions of the center of the spherical lens.

As the system employs QD sensors with small voltage signals as output signals, it is necessary to undergo calibration and conversion to obtain the calibration factor *K*. After obtaining the value of *K*, high-precision machine tools are utilized for the calibration of the 3D sensing module. This calibration involves entering standard coordinate displacements into the machine tool, sequentially moving in the *XYZ* directions, and comparing the differences between the input position signals and the 3D sensing module displacement signals. This process confirms the accuracy and precision of the sensing module. The calibration and comparison results are illustrated in Table 1.

After calibrating the 3D sensing module, it is installed on the CNC workstation. Next, the standard rod is mounted on the spindle of the CNC machine tool, ensuring that there is no eccentricity between the standard rod and the spindle, as shown in Fig. 2. The spindle is then rotated at a speed of 8000 rpm. Finally, the CNC machine tool is moved along the *XYZ* axes to

Fig. 1. (Color online) 3D sensing module and standard rod.[3]

Table 1
LASER R-TEST's calibration results with the spindle stopped.

	X		*Y*		*Z*	
Target value	Actual value	Residual	Actual value	Residual	Actual value	Residual
100	100.2	−0.2	99.6	0.8	100.6	−0.6
90	89.7	0.3	89.2	0.8	90.3	−0.3
80	79.6	0.4	79.2	0.8	80.1	−0.1
70	69.6	0.4	69.5	0.5	70.3	−0.3
60	59.7	0.3	59.5	0.2	60.5	−0.5
50	49.1	0.9	49.8	−0.1	50.6	−0.6
40	40.1	−0.1	40.1	−0.1	40.6	−0.6
30	30.1	−0.1	30.1	−0.1	30.8	−0.8
20	20.1	−0.1	19.9	0.1	20.5	−0.5
10	10	0	9.6	0.4	10.4	−0.4
0	0	0	0	0	0	0
−10	−9.6	−0.4	−10.7	0.7	−9.8	−0.2
−20	−19.7	−0.3	−20.5	0.5	−20.2	0.2
−30	−29.5	−0.5	−30.5	0.5	−29.9	−0.1
−40	−39.2	−0.8	−40.3	0.3	−30.9	−0.1
−50	−49	−1	−50.2	0.2	−49.7	−0.3
−60	−59.1	−0.9	−60	0	−59.5	−0.5
−70	−69	−1	−70.2	0.2	−69.9	−0.1
−80	−79.6	−0.4	−80.4	0.4	−80.3	0.3
−90	−90	0	−90.3	0.3	−90.8	0.8
−100	−100.1	0.1	−100.7	0.7	−101.1	1.1

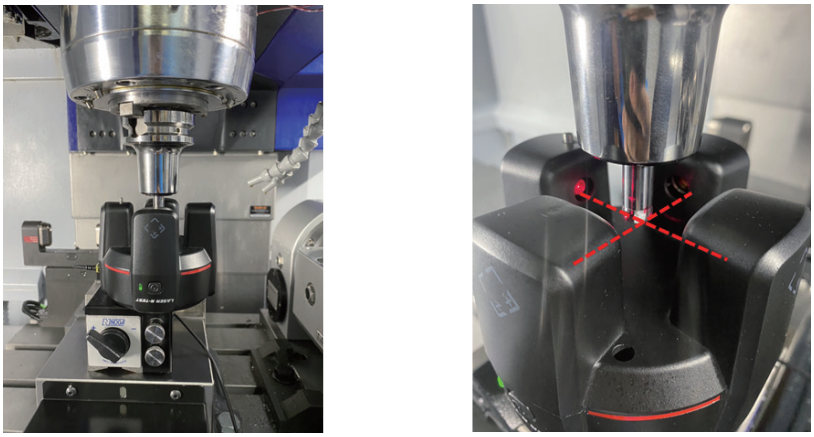

Fig. 2. (Color online) LASER R-TEST and tool holder setup.[1]

verify whether the 3D sensing module can accurately sense displacements in all three directions. The verification results are depicted in Table 2.

2.3 Placement location of PT100[1]

PT100 sensors were primarily used to measure temperature changes. These sensors were installed at different locations on the spindle components, motors and the machine tool structure.

Table 2
LASER R-TEST's calibration results during spindle rotation.

	X		*Y*		*Z*	
Target value	Actual value	Residual	Actual value	Residual	Actual value	Residual
100	99.9	0.1	99.9	0.1	100.9	−0.9
90	89.8	0.2	89.7	0.3	90.5	−0.5
80	79.3	0.7	79.5	0.5	80.2	−0.2
70	69.2	0.8	69.6	0.4	70.2	−0.2
60	59.3	0.7	59.6	0.4	60.2	−0.2
50	49.6	0.4	49.8	0.2	50.3	−0.3
40	39.9	0.1	39.8	0.2	40.5	−0.5
30	30.1	−0.1	29.6	0.4	30.7	−0.7
20	20.2	−0.2	19.6	0.4	20.7	−0.7
10	10.3	0.3	9.7	0.3	10.5	−0.5
0	0	0	0	0	0	0
−10	−9.6	−0.4	−10.6	0.6	−10.3	0.3
−20	−19.7	−0.3	−20.7	0.7	−20.4	0.4
−30	−29.5	−0.5	−30.6	0.6	−30.4	0.4
−40	−39.3	−0.7	−40.5	0.5	−40.1	0.1
−50	−49.3	−0.7	−50.4	0.4	−49.9	−0.1
−60	−59.3	−0.7	−60.3	0.3	−60	0
−70	−69.3	−0.7	−70.5	0.5	−70.1	0.1
−80	−79.8	−0.2	−80.4	0.4	−80.3	0.3
−90	−90.1	0.1	−90.5	0.5	−90.7	0.7
−100	−100.1	0.1	−100.5	0.5	−101.1	1.1

When the spindle rotates at a high speed, temperature changes at different locations are sensed. The correlation coefficient between spindle thermal error and temperature changes at different locations can then be established using the Spearman correlation coefficient and XGBoost. In this experiment, the sensors were placed at 13 positions on the machine, as shown in Fig. 3.(1)

3. Spindle Thermal Error Prediction

The approach involves installing PT100 sensors on the machine for temperature data collection. Data transmission is carried out through the serial port. Laser R-Test (LRT) is used for thermal error data collection, with signal transmission occurring over Wi-Fi. Subsequently, an edge computer is utilized for data collection, and AI models are established on the basis of the temperature, speed, and displacement data collected. The system framework diagram is shown Fig. 4.

The following parts will be introducing the essential steps of thermal error prediction, including data collection, XGBoost for sensor selection, data normalization, and algorithms used in the thermal compensation model.

3.1 Data collection

To assess the long-term accuracy of various neural network algorithms, we have designed an experimental method by testing the model with data recorded on 2022/07/17, then comparing it

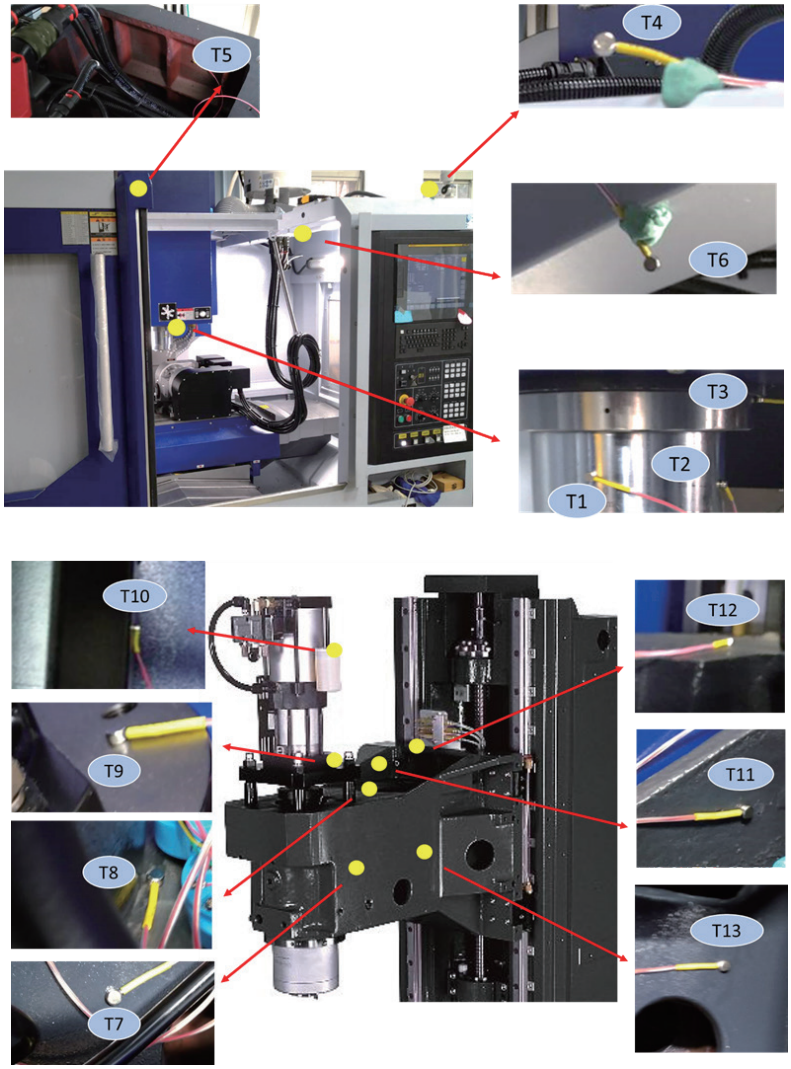

Fig. 3. (Color online) Locations of PT100 sensors.[1]

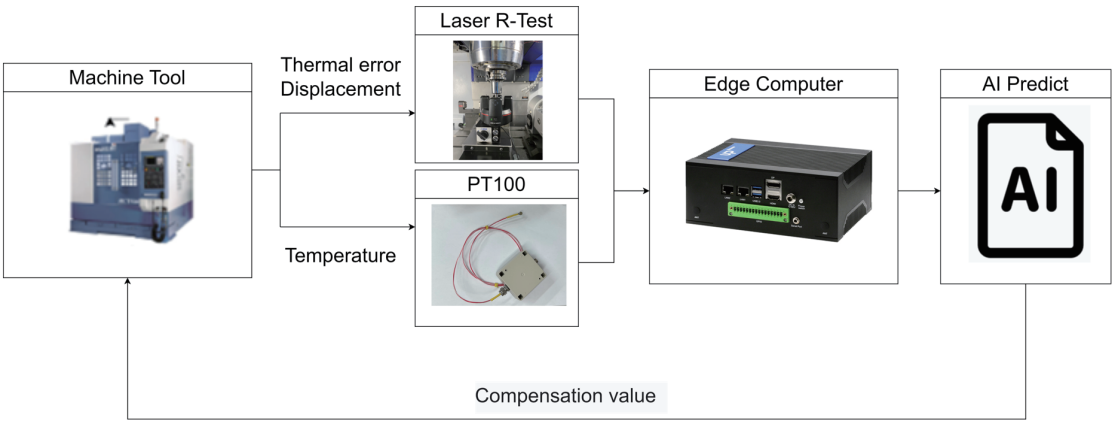

Fig. 4. (Color online) System framework diagram.

with data recorded one month later (2022/08/15) and six months later (2023/04/18). The data from 2022/07/17 was used for module testing and feature selection. Before establishing the thermal error model[1], it is necessary to identify the factors that affect thermal error. This study employs a CNC machine tool with a maximum spindle speed of 8000 RPM. To better simulate the actual machining process, various speed ratios were used in the experiments. It was observed that, compared with temperature changes, displacement changes exhibited a prominent and immediate response to different rotational speeds. Therefore, rotational speed was selected as an input parameter in this experiment. The selected speed and operating time are shown in Fig. 5, with a time span of 11 h from Figs. 5–7. It can be observed that when the spindle starts operating, both temperature and thermal error increase.

From the results shown in Fig. 7, it is observed that when the spindle rotates at a high speed and causes thermal error, the main directional errors at the tool tip point in the *Z*- and *Y*-directions are about 40–50 μm, while the error in the *X*-direction is 10 μm. The experimental results reveal that the phenomenon of thermal rise has the least impact on the *X*-direction of the

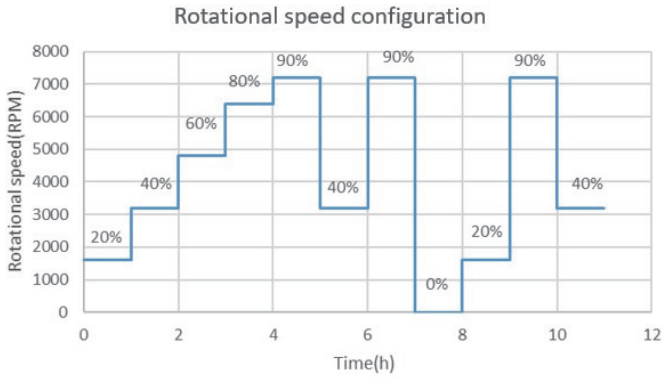

Fig. 5. (Color online) Spindle speed configuration.[1,8]

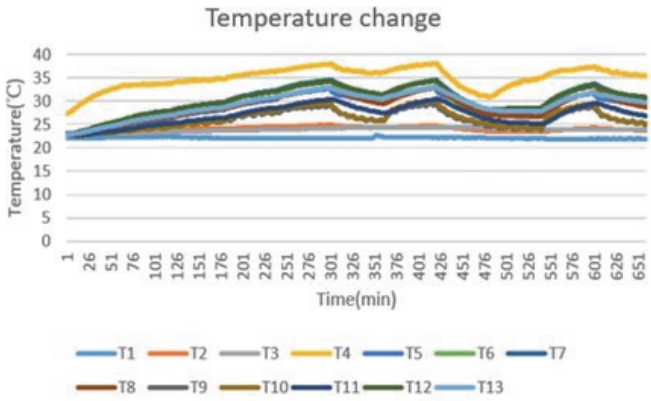

Fig. 6. (Color online) Temperature data.[1]

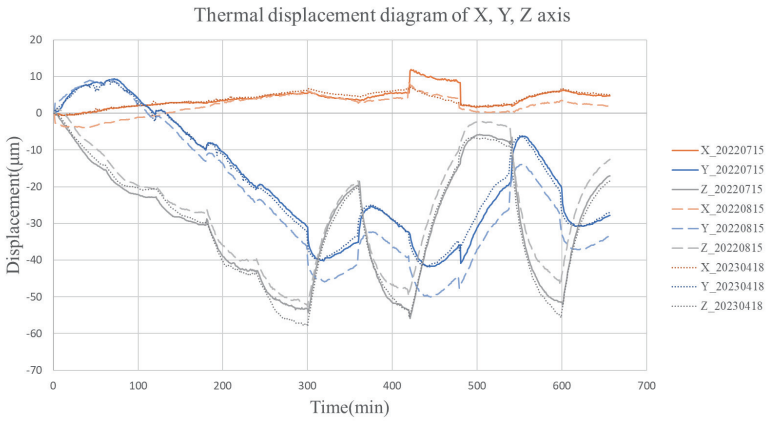

Fig. 7. (Color online) 11-h thermal error diagram of *X*-, *Y*-, and *Z*- directions.

CNC machine. Consequently, we initially focus on modeling the *Z*- and *Y*-directions, which are the primary directions of thermal rise errors, to establish the relationship between temperature and thermal rise errors. The *Y*-direction thermal error primarily stems from changes in the mechanical structure of the CNC machine, and thus, lacks repeatability, leading to a relatively poor prediction result. On the other hand, the thermal error in the *Z*-direction mainly arises from the thermal expansion deformation of the spindle. The thermal error of a single component tends to be more repeatable than the total thermal error of the machine structure.

3.2 Feature and sensor selection mechanism

In this study, we tested two selection mechanisms, the Spearman correlation coefficient and XGBoost, to select feature parameters that are highly correlated with thermal error and eliminate redundant parameters. The feature set from the experimental data was constructed, which includes temperature, spindle speed, and thermal displacement data. It can be observed from the results in Figs. 5–7 that compared with temperature changes, thermal displacement variations are very notable and immediate at different spindle speeds. The measurement results in Figs. 5–7 suggest that the spindle speed feature is very important in the thermal error model. Then, two selection mechanisms are used for feature analysis and sensor selection, comparing whether the analysis results match the measurement results. According to the Spearman correlation coefficient's feature analysis results shown in Fig. 8, we found that the correlation value between the spindle speed feature and thermal displacement is low. The result could lead to the removal of the spindle speed feature from future neural network models, which contradicts observations from the measurement results. However, as shown in Fig. 9, the XGBoost algorithm analysis highlighted the importance of the spindle speed feature in thermal displacement, aligning closely with the measurement results. Therefore, XGBoost was used to obtain the weight coefficients of each feature and sensor in this study; then, the optimal number and features for prediction were selected. This method of using XGBoost not only reduces the need for the sensor setup and model training time, but also effectively improves the accuracy of the thermal error model.

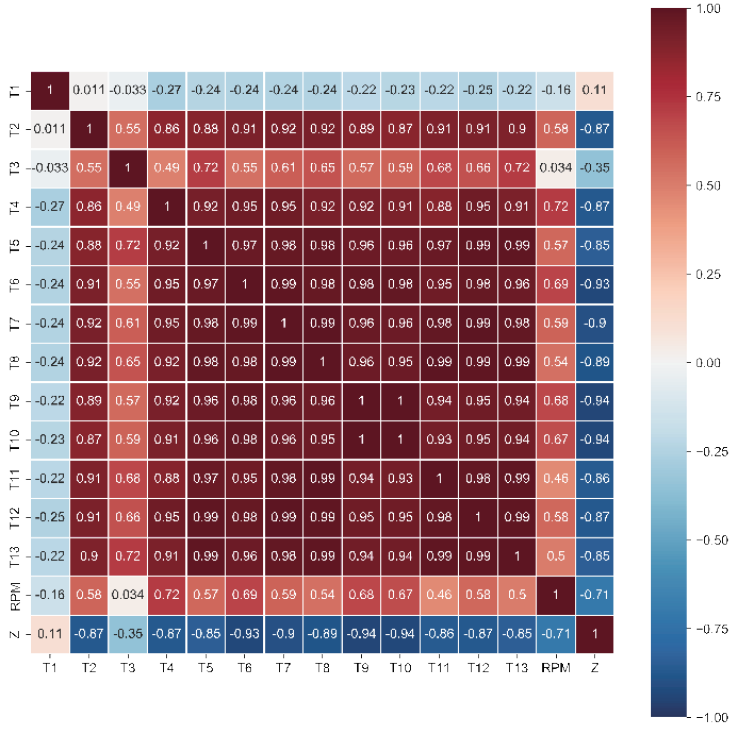

Fig. 8. (Color online) 2022/07/15_Spearman feature selection.

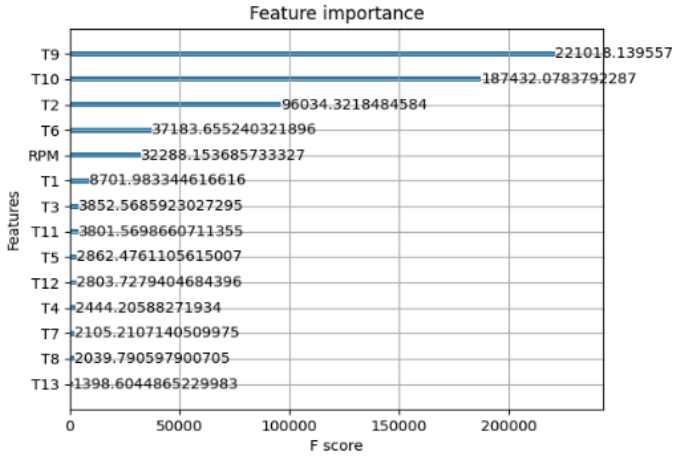

Fig. 9. (Color online) 2022/07/15_XGBoost feature selection.[1]

3.3 Normalization[1,24]

To eliminate the effects of units and dimensions, and make the model converge, data normalization is performed. For the temperature data, to ensure that the model can be applied to different temperature conditions, the minimum and maximum values of the temperature range were set at −20 and 100, respectively, then scaled proportionally to the range of 0 to 1, which is known as min-max normalization:

$$X_{nom} = \frac{X - X_{min}}{X_{max} - X_{min}} \in [0,1], \tag{1}$$

where X_{max} is the maximum value and X_{min} is the minimum value.

In this study, the thermal error is normalized to a range from 100 to 100 μm. The choice of this range is primarily because most CNC spindle thermal errors fall within this interval. To enhance the generalizability of subsequent data, we normalize all data on the basis of the same standard.

3.4 Neural network model[1]

In this section, we introduce four types of neural network models used in this study: TCN, GAN, LSTM, and BiLSTM. We first introduce TCN, which is a CNN variant that combines the architectures of RNN and CNN. The structure diagram of the TCN is shown in Fig. 10. The simple convolutional structure allows it to perform better than typical RNNs (such as LSTM) when it comes to multiple tasks and data, and it also exhibits longer effective memory.[1,25–27] Causal convolution is used in TCN, which defines that the output is only affected by past data instead of future data, and has memory of the past. In addition, the fully connected layer ensures that the input and output dimensions are the same.

Second, GAN uses two neural networks, a generator and a discriminator, which compete against each other in a game. The generator learns to generate new data with the same statistics as the training set to fool the discriminator, whereas the discriminator learns to assess realities and fakes to win the game.

Third, LSTM is a type of RNN capable of learning long-term dependences. It contains an internal cell state that flows through time, allowing it to bridge longer gaps than conventional RNNs without forgetting earlier inputs. Lastly, BiLSTM combines the characteristics of LSTM

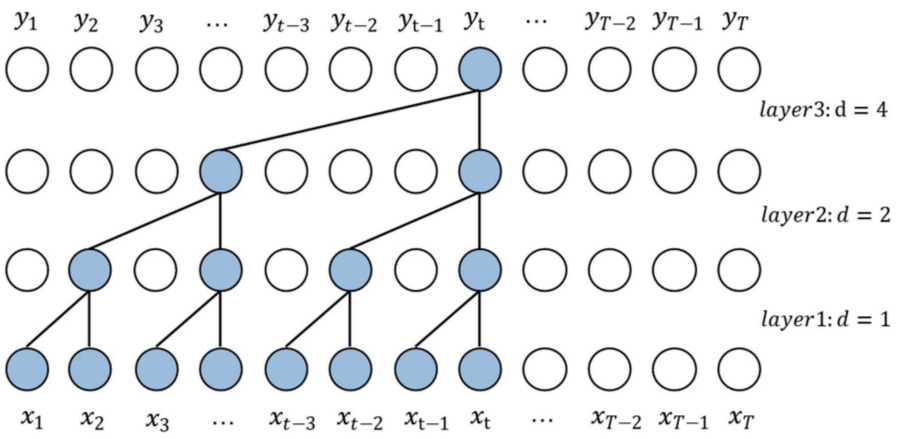

Fig. 10. (Color online) TCN structure diagram.[26]

and bi-directional RNN. It consists of two LSTM layers, one processing data from left to right and the other from right to left. BiLSTM is capable of simultaneously considering past and future information, enabling more precise predictions of temperature changes and thermal errors. This model is particularly effective in capturing dynamic changes in factors such as processing time and ambient temperature, thereby enhancing prediction accuracy. The structure diagram of BiLSTM is shown in Fig. 11.

We conducted hyperparameter tuning through random grid search. The hyperparameters under consideration for tuning included the number of neurons, learning rate, the number of epoch, batch size, and the type of optimizer, as shown in Table 3. For each hyper parameter, various types and values were listed, and then random selection and arrangement were performed for prediction. The best hyper parameter combination was determined by comparing prediction results.

4. Experiment and Model Prediction Results

In this study, the input data consists of 14 signals in total: 13 temperature data points collected from the PT100 module and one spindle speed data.[1] The measurement experiments showed that the thermal errors are mainly observed in the *Z*- and *Y*-directions. These signals can be acquired using LASER R-TEST developed in this study, and the data sampled on July 15, 2022 was utilized as the training and validation dataset, including 19800 single-featured data points with an output frequency of two times per second. The data covered an 11-h duration of varying spindle speed. Subsequently, datasets one month after (2022/8/15) and six months after (2023/04/08) were used as the testing set to assess the long-term accuracy of the model.

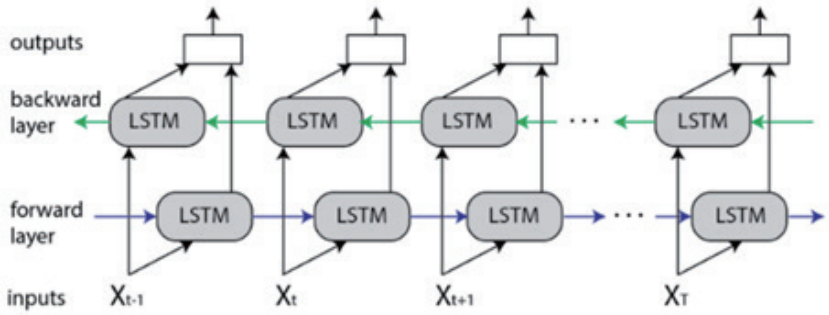

Fig. 11. (Color online) BiLSTM structure diagram.[28]

Table 3
Hyperparameter tuning of models.

	Number of layers	Learning rate	Number of epoch	Batch size	Type of optimizer
TCN	1	0.001	100	128	Adam
LSTM	2	0.001	100	128	Adam
GAN	2	0.001	100	160	Adam
BiLSTM	2	0.001	100	128	Adam

In this research, we tested various commonly used machine learning algorithms such as TCN, LSTM, GAN, and BiLSTM. The aim was to evaluate the accuracy of different AI models with different feature parameters over an extended period. According to Table 4, the correlation coefficients between each temperature sensor and thermal error in the *Y*- and *Z*-directions of the spindle can be identified. The correlation coefficient is lower for the *Y*-direction of the spindle than for the *Z*-direction since thermal errors in the *Y*-direction are primarily affected by structural deformation and temperature rise. The correlation coefficient for the key parameter, which is the spindle speed, is only about 0.2, indicating that it may be excluded during feature selection. However, on the basis of previous experience and research, we understand that variations in spindle speed are important factors that affect spindle temperature rise. Therefore, we attempted to incorporate this factor into the model and found that it indeed resulted in better performance, with a 20% improvement. Table 5 indicates that most prediction results in higher *Z*-direction achieve an accuracy of more than 70% and an error range of less than 20 μm. The *Y*-direction prediction is poor since the thermal errors involve both structural and spindle thermal deformation errors. Moreover, the structure may have changed after six months of waiting. Therefore, to achieve higher prediction results for the *Y*-direction thermal error in the future, we may consider adding more temperature sensors at places such as on the lead screw of the drive system and on the *Z*-axis mounting surface to detect thermal errors resulting from structural deformations. The residuals of prediction results in the *Z*- and *Y*-directions are shown in Tables 5 and 6.

Overall, TCN produced residuals that were lower and more consistent than those produced by both the LSTM and GAN models across different datasets and numbers of sensors, indicating superior stability in forecasting time series data. As the number of sensors decreased, the prediction accuracy declined for all models, although the decline amplitude was smaller for TCN than for LSTM and GAN. The use of a temporal convolutional structure in TCN enables the more effective capture of long-term dependences.

Table 4
Order of parameters in each direction.

Z-direction													
Number of parameters	Order of parameters												
14	T9, T10, T2, T6, RPM, T1, T3, T11, T5, T12, T4, T7, T8, T13												
10	T9, T10, T2, T6, RPM, T1, T3, T11, T5, T12												
7	T9, T10, T2, T6, RPM, T1, T3												
Y-direction													
Number of parameters	Order of parameters												
14	T3, T11, T13, T5, T8, T12, T7, T2, T10, T6, T9, T4, RPM, T1												
10	T3, T11, T13, T5, T8, T12, T7, T10, T6, RPM												
7	T3, T11, T13, T5, T8, T12, RPM												
Correlation coefficient													
	T1	T2	T3	T4	T5	T6	T7	T8	T9	T10	T11	T12	T13
Y-direction	0.26	0.65	0.87	0.42	0.66	0.51	0.60	0.65	0.53	0.53	0.71	0.63	0.70
Z-direction	0.22	0.81	0.24	0.85	0.83	0.93	0.90	0.88	0.92	0.92	0.85	0.86	0.84

Table 5
Residuals of prediction results in *Z*-direction.

		2022/08/15 prediction result			2023/04/18 prediction result		
Number of sensor inputs		Actual thermal error (μm)	Residual of prediction (μm)	Improved efficiency (%)	Actual thermal error (μm)	Residual of prediction (μm)	Improved efficiency (%)
TCN	14	54.52	11.669	78.597	58.46	14.55	75.11
	10		12.617	76.858		15.26	73.9
	7		14.718	73.004		16.78	71.3
LSTM	14		15.436	71.687		10.7	81.7
	10		16.827	69.136		12.06	79.37
	7		15.497	71.576		14.19	75.73
GAN	14		12.962	76.276		14.80	74.622
	10		16.865	69.051		16.61	71.598
	7		16.498	69.763		19.51	66.610
BiLSTM	14		7.94	85.44		11.72	79.95
	10		10.33	81.05		12.88	77.97
	7		16.83	69.13		14.22	75.68

Table 6
Residuals of prediction results in *Y*-direction.

		2022/08/15 prediction result			2023/04/18 prediction result		
Number of sensor inputs		Actual thermal error (μm)	Residual of prediction (μm)	Improved efficiency (%)	Actual thermal error (μm)	Residual of prediction (μm)	Improved efficiency (%)
TCN	14	59.09	26.92	54.44	50.94	10.78	78.82
	10		18.22	69.17		12.27	75.88
	7		27.19	53.98		20.32	60.06
LSTM	14		23.51	60.21		16.37	67.83
	10		24.48	58.57		20.65	59.41
	7		20.22	65.79		23.31	49.59
GAN	14		24.08	59.208		18.58	57.18
	10		23.96	59.512		26.77	47.456
	7		25.88	56.229		28.03	45.088
BiLSTM	14		19.11	67.66		14.81	70.81
	10		20.14	65.92		18.65	63.34
	7		24.23	58.99		19.74	61.21

GAN's generator–discriminator relationship causes instability and inability to model complex time series distributions, resulting in the largest residual among the three models. Thus, the variation in models' performance could be reasonably attributed to differences in their network architecture designs and how well suited each is for solving time series problems. Tables 5 and 6 further show the average prediction results of the three models for 2022/8/15 and 2023/04/08. Figures 12–20 then show the output graphs of prediction results, with GAN oscillating the most. BiLSTM, with its bi-directional LSTM layers, can simultaneously consider both past and future information. The outputs of these two LSTM layers are combined; therefore, in the results presented above, BiLSTM can provide a comprehensive time series analysis when the data is complete, significantly improving prediction accuracy. This approach enhances the model's adaptability to complex variations.

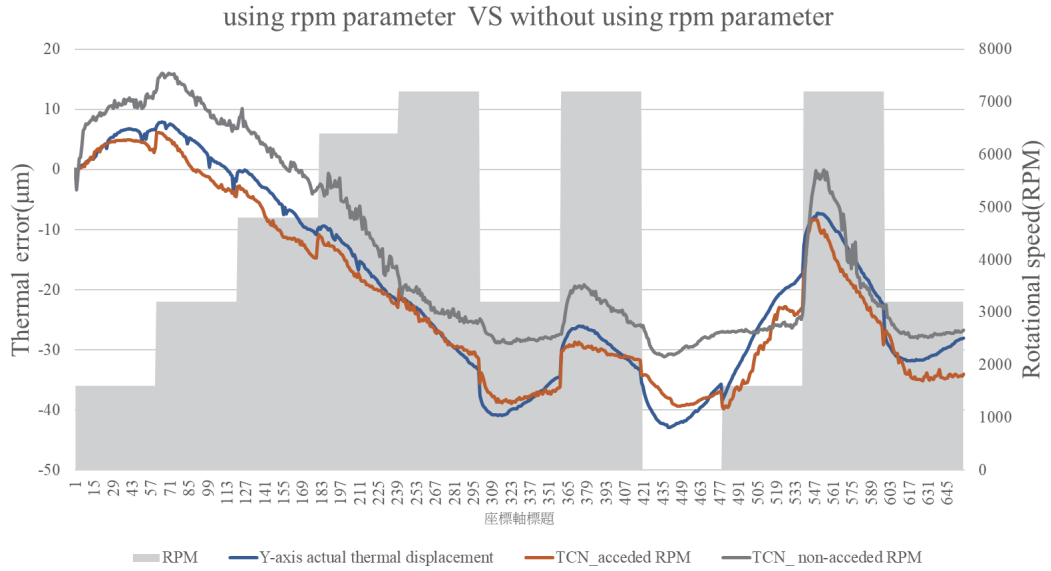

Fig. 12. (Color online) Comparing prediction results with and without using rpm parameter.

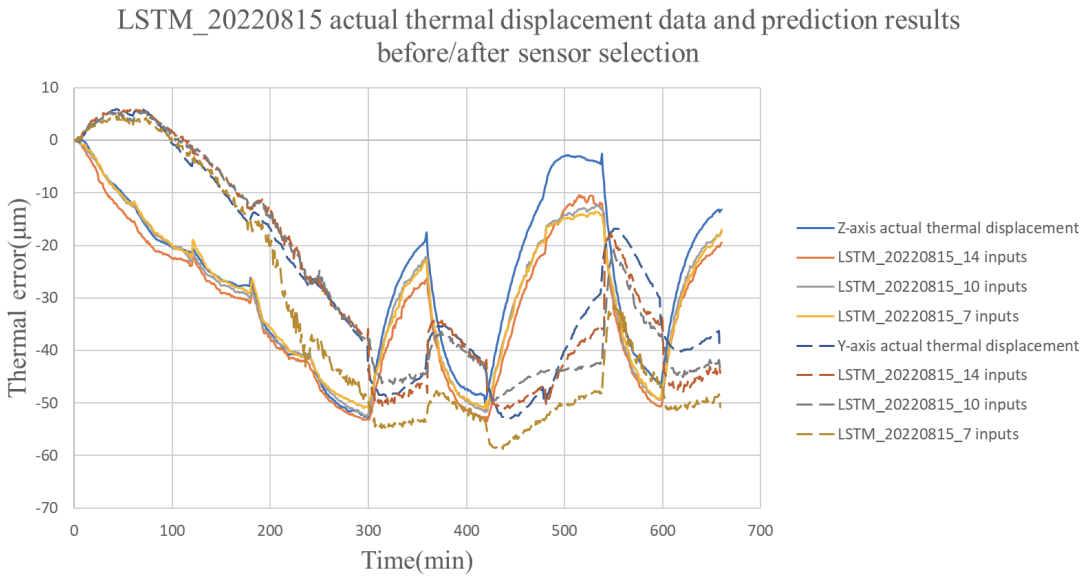

Fig. 13. (Color online) LSTM_20220815 actual thermal error data and prediction results before/after sensor selection.

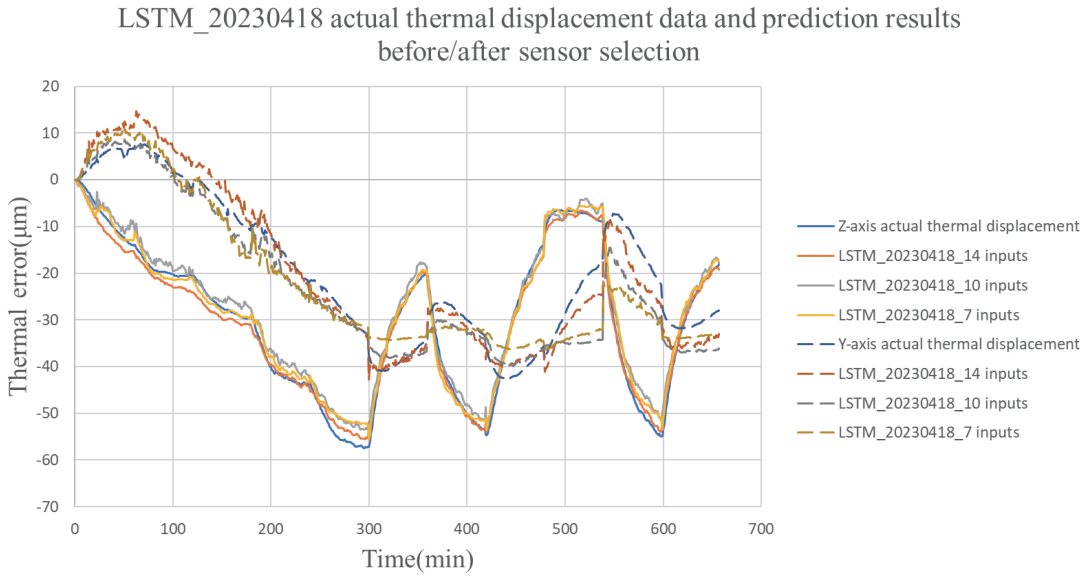

Fig. 14. (Color online) LSTM_20230418 actual thermal error data and prediction results before/after sensor selection.

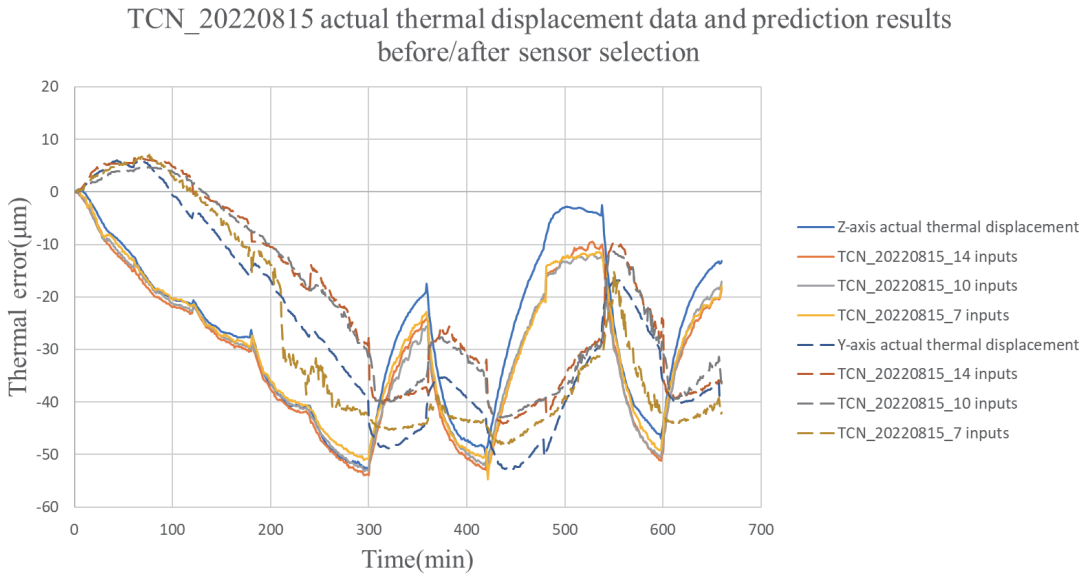

Fig. 15. (Color online) TCN_20220815 actual thermal error data and prediction results before/after sensor selection.

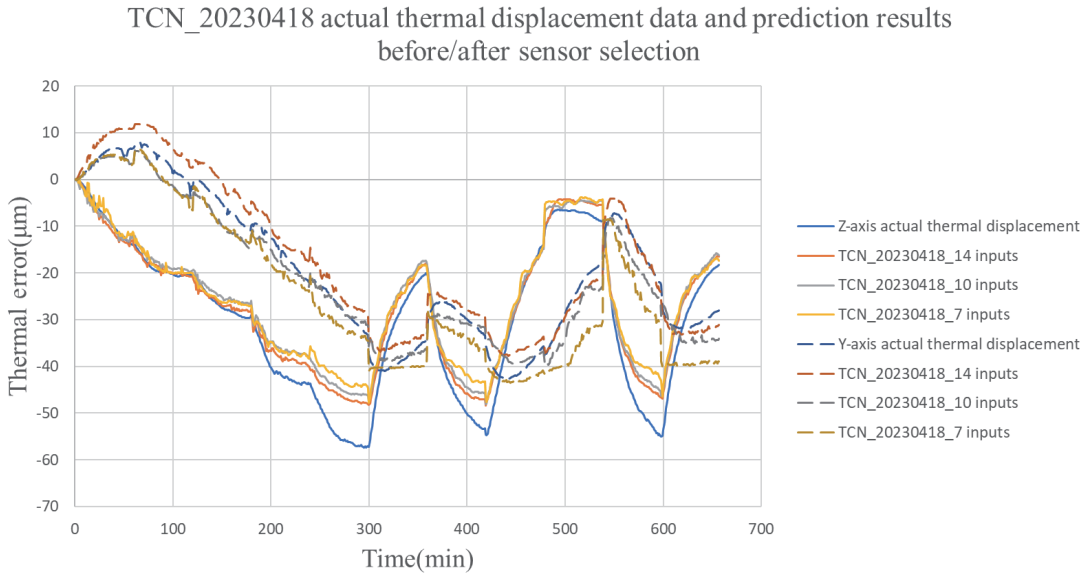

Fig. 16. (Color online) TCN_20230418 actual thermal error data and prediction results before/after sensor selection.

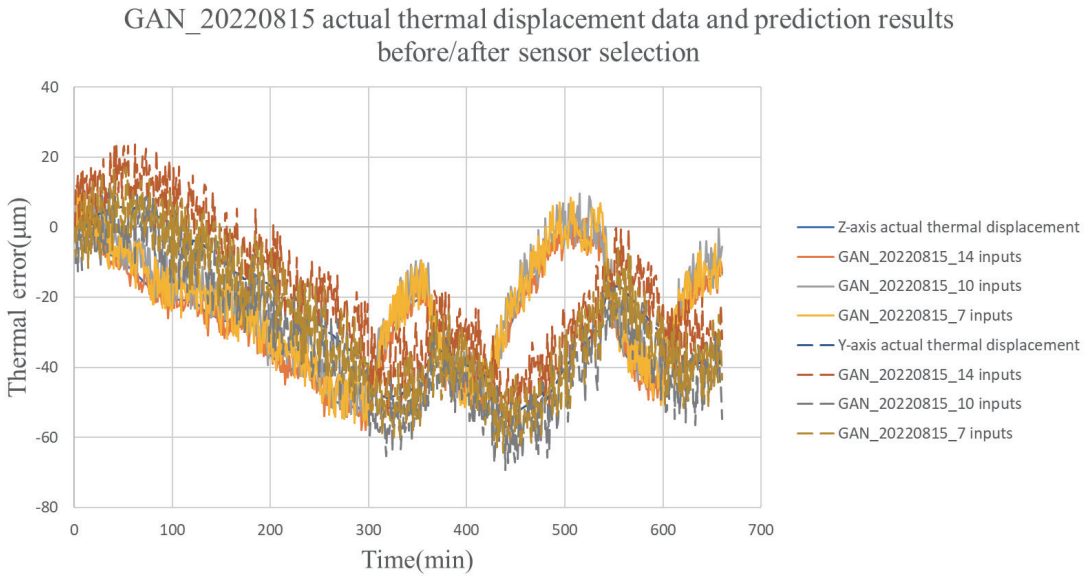

Fig. 17. (Color online) GAN_20220815 actual thermal error data and prediction results before/after sensor selection.

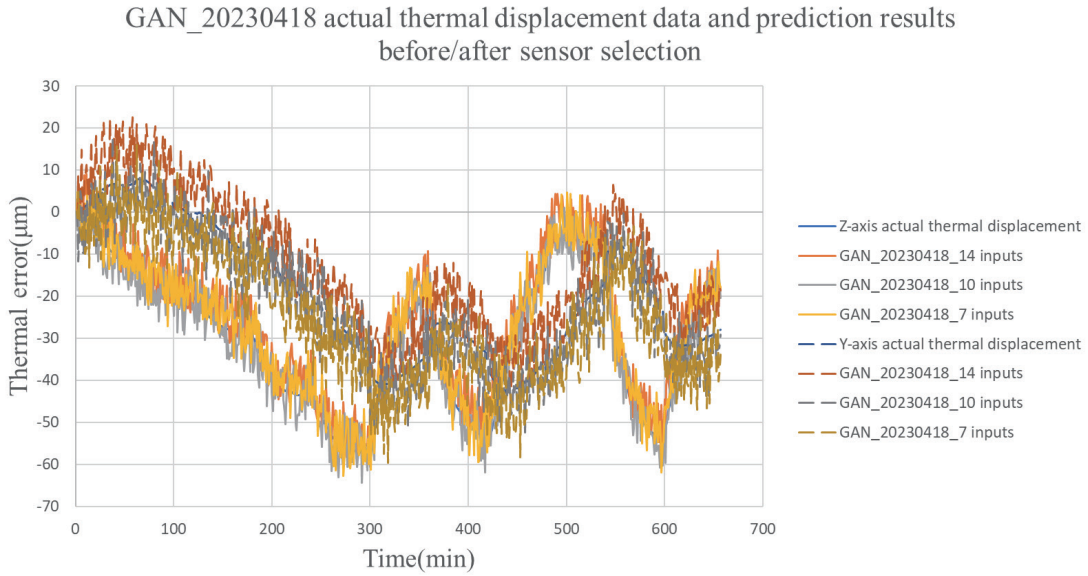

Fig. 18. (Color online) GAN_20230418 actual thermal error data and prediction results before/after sensor selection.

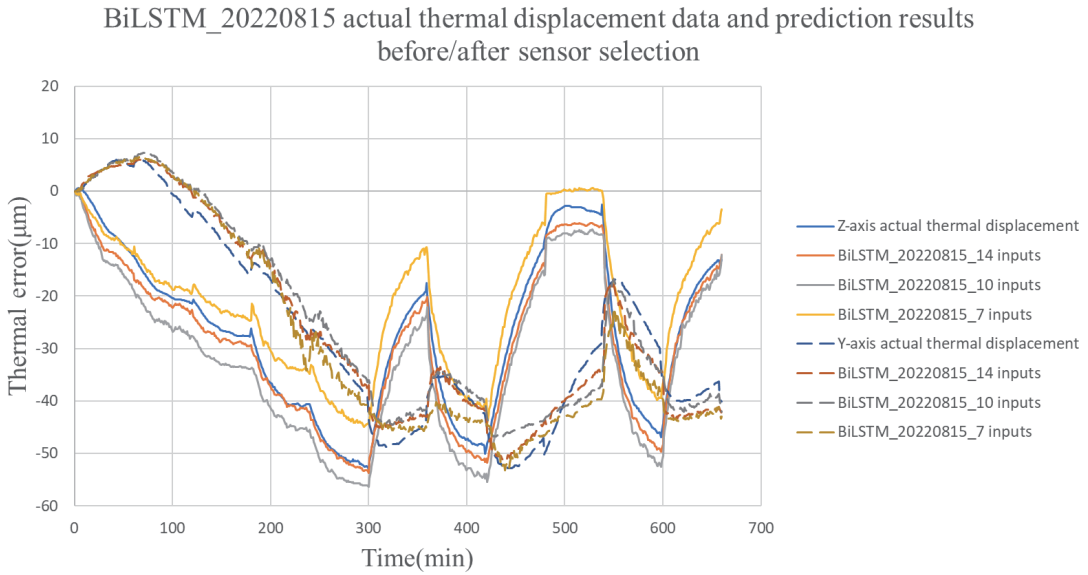

Fig. 19. (Color online) BiLSTM_20220815 actual thermal error data and prediction results before/after sensor selection.

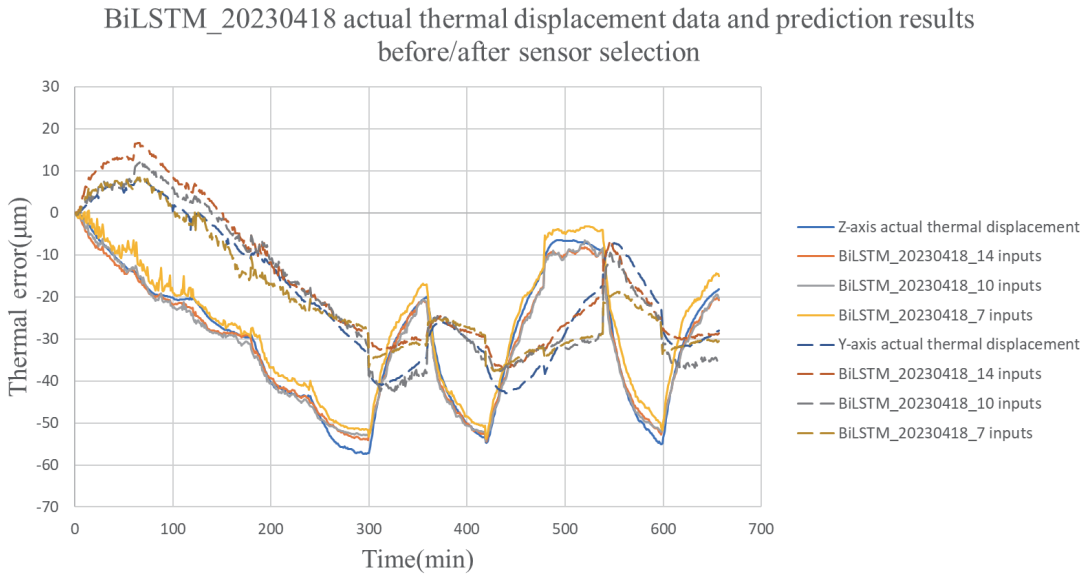

Fig. 20. (Color online) BiLSTM_20230418 actual thermal error data and prediction results before/after sensor selection.

5. Conclusions

We successfully developed LASER R-TEST using laser light sources, QD, and ball lenses. This system can accurately measure the thermal error in the *XYZ* direction during spindle rotation. Furthermore, we developed a temperature sensing module and introduced neural network algorithms such as LSTM, TCN, GAN, and BiLSTM to establish an AI model correlating temperature sensing signals with thermal errors.

According to the experimental results, we found that with 14 input parameters, various models could achieve a prediction accuracy between 70 and 85% in the *Z*-direction. In this investigation, XGBoost was introduced as a feature selection mechanism, aiming to reduce the number of future sensor installations and associated costs, and identify truly key parameter factors. According to the experimental results, when the number of sensors was reduced from 14 to 7, the prediction accuracy of the AI model could be maintained above 70% in the *Z*-direction. In terms of prediction accuracy in the *Y*-direction, the current accuracy is approximately between 60 and 70%, which is lower than that in the *Z*-direction, since *Y*-direction thermal errors mostly result from mechanical structure changes and the lack of repeatability. Additionally, after six months, there is a significant decline in the model's prediction accuracy, possibly owing to the machine structure being more substantially affected by varying environmental temperatures. Through several months of data testing and training, this method was proven to satisfy adaptability in six months. The experimental results demonstrate that the BiLSTM model exhibits greater stability and longer temporal effectiveness than the other models.

In the future, in the case of improving model failure, a pre-trained model can be established using TCN and BiLSTM. Once a model failure is detected or when the prediction performance deteriorates, transfer learning can be employed to fine-tune the model. This approach reduces the reliance on large amounts of labeled data and accelerates the training process.

Acknowledgments

This paper is based on National Science and Technology Council project number MOST 111-2218-E-002-033-. The authors would like to express their sincere gratitude to the Ministry of Science and Technology, members of the Smart Machinery and Intelligent Manufacturing Research Center at NFU, and the Ministry of Economic Affairs "Application of 5G Industrial Internet of Things to Promote Digital Transformation of CNC Machine Tool Industry and Cloud Value-added Service Plan" for their assistance. Also, the authors would like to express their sincere gratitude to Dr. Wen-Yuh Jywe for providing experimental equipment.

References

1 T. H. Hsieh, W. Y. Jywe, H. Y. Lai, Y. H. Chou, and T. H. Wu: 2023 6th Int. Symp. Computer, Consumer and Control (IS3C, 2023) 5. https://doi.org/10.1109/IS3C57901.2023.00010
2 C. S. Tran, T. H. Hsieh, and W. Y. Jywe: Appl. Sci. **11** (2021) 9507. https://www.mdpi.com/2076-3417/11/20/9507
3 Optical detecting apparatus for detecting a degree of freedom error of a spindle and a detecting method thereof: https://patents.google.com/patent/EP3392609A1/en (accessed August 2023).
4 W. Y. Jywe, T. H. Hsieh, J. M. Hsu, Y. W. Chang, S. Y. Huang, J. Y. Chiu, P. W. Lu, and J. J. Tseng: J. Mechatronic Industry **468** (2022) 20. https://www.airitilibrary.com/Article/Detail?DocID=P20171221002-202203-202203010014-202203010014-20-27
5 Y. S. Lu, T. W. Liu, M. Q. Hong, and M. S. Tsai: Instrum. Today **221** (2019) 56. https://www.airitilibrary.com/Article/Detail?DocID=10195440-201912-201912300016-201912300016-56-70
6 C. Y. Zheng, G. D. Zhou, and D. K. Liu: Eng. Mech. **38** (2021) 68. https://doi.org/10.6052/j.issn.1000-4750.2020.05.0323
7 J. L. Liu, C. Ma, H. Q. Gui, and S. L. Wang: Appl. Soft Comput. **102** (2021) 107094. https://doi.org/10.1016/j.asoc.2021.107094
8 Y. L. Chen: Using Laser R-Test to Develop Artificial Intelligence Thermal Temperature Rise Compensation System (Department of Automation Engineering Master's Thesis, Taiwan, 2021). https://hdl.handle.net/11296/3855nr
9 Y. C. Liu, K. Y. Li, and Y. C. Tsai: Appl. Sci. **11** (2021) 5444. https://doi.org/10.3390/app11125444
10 P. L. Liu, Z. C. Du, X. B. Feng, M. Deng, and J. G. Yang: Adv. Manuf. **9** (2021) 235. https://doi.org/10.1007/s40436-020-00342-x
11 P. F. Zhang, Z. L. Fang, L. Y. Li, and T. T. Yang: J. Sens. **2023** (2023). https://doi.org/10.1155/2023/6616607
12 J. Yoon, D. Jarrett, and M. Van Der Schaar: 33rd Conf. Neural Information Processing Systems (NerIPS, 2019).
13 J. L. Wu, X. R. Tang, and C. H. Hsu: Soft Comput. **27** (2023) 8209. https://doi.org/10.1007/s00500-022-07716-2
14 S. Ravuri, K. Lenc, M. Willson, D. Kangin, R. Lam, P. Mirowski, M. Fitzsimons, M. Athanassiadou, S. Kashem, S. Madge, R. Prudden, A. Mandhane, A. Clark, A. Brock, K. Simonyan, R. Hadsell, N. Robinson, E. Clancy, A. Arribas, and S. Mohamed: Nature **597** (2021) 672. https://doi.org/10.1038/s41586-021-03854-z
15 G. Jia, X. Zhang, X. Wang, X. Zhang, and N. Huang: Int. J. Adv. Manuf. Technol. **127** (2023) 1525. https://doi.org/10.1007/s00170-023-11616-6
16 P. H. Kuo, Y. W. Chen, T. H. Hsieh, W. Y. Jywe, and H. T. Yau: IEEE Sens. J. **23** (2023) 12574. https://doi.org/10.1109/JSEN.2023.3269064
17 F. Tan, G. Yin, K. Zheng, X. Wang, and X. Ma: Lubricants **11** (2023) 343. https://doi.org/10.3390/lubricants11080343
18 J. Chen and X. Wang: 2021 IEEE 4th Advanced Information Management, Communicates Electronic and Automation Control Conf. (IMCEC, 2021) 324. https://doi.org/10.1109/IMCEC51613.2021.9482246

19 G. Yin, F. Tan, K. Zheng, and X. Wang: Int. J. Adv. Manuf. Technol. **116** (2021) 99. https://doi.org/10.1007/s00170-021-07066-7
20 Q. Guo, S. Fan, R. Xu, X. Cheng, G. Zhao, and J. Yang: Chin. J. Mech. Eng. **30** (2017) 746. https://doi.org/10.1007/s10033-017-0098-0
21 C. Wu, S. Xiang, and W. Xiang: J. Manuf. Syst. **59** (2021) 67. https://doi.org/10.1016/j.jmsy.2021.01.013
22 G. Li, X. Tang, Z. Li, K. Xu, and C. Li: Precis. Eng. **73** (2022) 140. https://doi.org/10.1016/j.precisioneng.2021.08.021
23 C. Chen, H. Dai, C. Lee, T. H. Hsieh, W. Hung, and W. Y. Jywe : Int. J. Adv. Manuf. Technol. **130** (2024) 2423. https://doi.org/10.1007/s00170-023-12778-z
24 Database Systems: The Complete Book: https://www.db-book.com
25 P. Wu, J. Sun, X. Chang, W. Zhang, R. Arcucci, Y. Guo, and C. C. Pain: Comput. Methods Appl. Mech. Eng. **360** (2020) 112766. https://doi.org/10.1016/j.cma.2019.112766
26 W. Sheng, K. Liu, D. Jia, S. Chen, and R. Lin: Energies **15** (2022) 5584. https://doi.org/10.3390/en15155584
27 M. Huang, X. Xie, W. Sun, and Y. Li: Lubricants **12** (2024) 36. https://doi.org/10.3390/lubricants12020036
28 T. Ho, H. M. Bui, and T. K. Phung: Int. J. Advances in Intelligent Informatics **9** (2023) 273. https://doi.org/10.26555/ijain.v9i2.976

About the Authors

Tung-Hsien Hsieh received his M.S. degree from the Department of Mechanical and Electro-Mechanical Engineering, National Formosa University, Yunlin, Taiwan, in 2006, and his Ph.D. degree from the Institute of Manufacturing Information Systems, National Cheng Kung University, Tainan, Taiwan in 2011. He is currently an assistant professor in the Department of Automation Engineering and a research fellow in the Smart Machinery and Intelligent Manufacturing Research Center at National Formosa University, Taiwan. He won the Young Researcher Award during the 7th International Conference of the Asian Society for Precision Engineering and Nanotechnology in 2017 and the Research Award from National Formosa University for three consecutive years. His major research interests include optical precision measurement, the compensation of machine tools, and automation engineering.

Hsin-Yu Lai received his B.S. degree in automation engineering from National Formosa University, in Taiwan, in 2023. He is currently pursuing his M.S. degree in the Department of Automation Engineering, and he is also a research assistant in Smart Machinery and Intelligent Manufacturing at National Formosa University, Taiwan. His research interests include precision measurement. (40827203@gm.nfu.edu.tw)

Yi-Hao Chou received his B.S. degree from the Department of Automation Engineering of National Formosa University, Taiwan, in 2023. He is currently pursuing his M.S. degree in mechanical engineering at National Taiwan University. His research interests include Internet of Things, precision measurement, and sensors. (40827210@gm.nfu.edu.tw)

Tsai-Hsu Wu received her B.S. degree in mechanical engineering from National Taiwan University (NTU), Taipei, Taiwan, in 2023. Her research interests include mechanism design and robotics. (b08502101@ntu.edu.tw)